Research Article Vol. 2, No. 5 / 15 May 2019 / OSA Continuum 1693

Ultra-multiplex CARS spectroscopic imaging with 1-millisecond pixel dwell time

HIDEAKI KANO,[1,2,3,*] TAKUMI MARUYAMA,[1] JUNKO KANO,[4] YUKI OKA,[5] DAIKI KANETA,[5] TIFFANY GUERENNE,[6] PHILIPPE LEPROUX,[4,7] VINCENT COUDERC,[7] AND MASAYUKI NOGUCHI[8]

[1]*Department of Applied Physics, Graduate School of Pure and Applied Sciences, University of Tsukuba, 1-1-1 Tennodai, Tsukuba, Ibaraki 305-8573, Japan*
[2]*Institute of Applied Physics, University of Tsukuba, 1-1-1 Tennodai, Tsukuba, Ibaraki 305-8573, Japan*
[3]*Tsukuba Research Center for Energy Materials Science (TREMS), University of Tsukuba, 1-1-1 Tennodai, Tsukuba, Ibaraki 305-8571, Japan*
[4]*LEUKOS, 37 Rue Henri Giffard, 87280 Limoges, France*
[5]*College of Engineering Sciences, University of Tsukuba, 1-1-1 Tennodai, Tsukuba, Ibaraki 305-8573, Japan*
[6]*PEIRENE, EA 7500, University of Limoges, 123 Avenue Albert Thomas, 87060 Limoges, France*
[7]*Institut de Recherche XLIM, UMR CNRS No. 7252, 123 Avenue Albert Thomas, 87060 Limoges CEDEX, France*
[8]*Department of Diagnostic Pathology, Faculty of Medicine, University of Tsukuba, 1-1-1 Tennodai, Tsukuba, Ibaraki 305-8575, Japan*
[*]*hkano@bk.tsukuba.ac.jp*

Abstract: We performed ultra-multiplex coherent anti-Stokes Raman scattering (CARS) spectroscopic imaging by using a CCD camera with a fast readout time (<1 ms). The ultra-multiplex CARS signal of a polystyrene bead was detected in the range 600–3600 cm^{-1} with resolution <10 cm^{-1}. The pixel dwell time was approximately 1 ms, which was limited by the readout time of the CCD camera rather than the exposure time. CARS images of 161×161 pixels were obtained of the polymer beads with a total data-acquisition time of approximately 28 s even with the use of a cost-effective microchip laser source. Label-free and ultra-multiplex (18 colors) imaging of living cells was also performed with an effective exposure time of 1.8 ms based on the molecular fingerprint as well as the C-H and O-H stretching vibrational modes using a master oscillator fiber amplifier laser source.

1. Introduction

Lately, *spectroscopic imaging* has attracted much attention, in particular in the field of coherent Raman imaging [1–4]. In comparison with spectral imaging, by which multiple wavelength-dependent images are obtained, spectroscopic imaging aims to achieve the vibrational-mode-dependent deconvolution of images with spectral data sets. The use of spectroscopic imaging has become prominent for coherent or nonlinear Raman imaging methods [1–9], among which coherent anti-Stokes Raman scattering (CARS) and stimulated Raman scattering (SRS) are two methods that are often used. Based on the CARS and SRS imaging techniques, several kinds of spectroscopic imaging have been reported, such as the multiplex method [10–16], laser-wavelength-scanning method [17–19], spectral focusing method [20], FT-CARS [21–23], and dual-comb method [24]. The multiplex method [10–14] utilizes a multi-channel detector such as a CCD or C-MOS camera with a spectrometer to cover the broad spectral range of the coherent Raman signal. The use of a broadband laser source such as a supercontinuum (SC) light source [16,25] or a femtosecond laser source [26] enables the typical spectral coverage of the multiplex CARS signal to reach approximately 3000 cm^{-1}, which is sufficiently broad to

#359178 https://doi.org/10.1364/OSAC.2.001693
Journal © 2019 Received 1 Feb 2019; revised 11 Apr 2019; accepted 14 Apr 2019; published 26 Apr 2019

OSA CONTINUUM

detect all the vibrational fundamental modes including the fingerprint region as well as the C-H and O-H stretching regions (ultra-multiplex CARS spectroscopic imaging). In particular, SC generation [12,13] has been achieved by using tapered fibers [12] and photonic crystal fibers (PCFs) [13].

Owing to the high peak power of the laser source, we are not only able to obtain the CARS signal but also other signals resulting from different nonlinear optical processes such as second harmonic generation (SHG), third harmonic generation (THG), and two-photon excitation fluorescence (TPEF), thereby enabling multi-modal nonlinear optical (or multi-photon) imaging [27–29]. We previously used multi-modal nonlinear optical imaging to successfully elucidate that the Rootletin filaments [30] of the rootlets in the retina are SHG-active [31].

Improving the detection speed of multiplex CARS imaging would require the specification of the laser source and multi-channel detector to be optimized. In the present study, living-cell imaging was performed using a SC source pumped by a master oscillator fiber amplifier (MOFA) [32] combined with a new CCD camera with high sensitivity and high-speed read-out. In the course of the study, we found that the new CCD camera allowed us to perform high-speed ultra-multiplex CARS imaging using a low-cost SC source pumped by a microchip laser.

2. Methods

2.1. Ultra-multiplex CARS spectroscopic imaging system

As shown in Fig. 1, two laser sources were incorporated in the experimental setup. The first source is based on a master oscillator fiber amplifier (MOFA) configuration, involving a microchip oscillator and a Yb-doped fiber amplifier (SM-1000, Leukos, France, custom-made). The microchip oscillator is a passively Q-switched laser comprising a Nd:YVO_4 crystal bonded with a saturable absorber mirror and pumped at 808 nm. The fiber amplifier is based on a two-stage configuration including a pre-amplifier and a booster using a polarization-maintaining, large-mode-area, double-clad Yb-doped fiber. The wavelength, temporal duration, repetition rate, and output average power of the MOFA laser source were 1064 nm, 85 ps, and 0.82 MHz, and ~2 W, respectively. The second laser source is a passively Q-switched microchip Nd:YAG laser (Leukos, Limoges, France). The wavelength, temporal duration, repetition rate, and output average power of the source were 1064 nm, 800 ps, 33 kHz, and ~300 mW, respectively; the specification are similar that used in [33]. The two laser sources can be switched based on the sample used in the experiments.

The laser pulses are divided in two with one part being used as the pump radiation (ω_1) for the CARS process and the other being seeded into a PCF to generate an SC, which is used as the Stokes radiation (ω_2) for the CARS process. The SC radiation is collimated by an off-axis parabolic mirror (RC04APC-P01, Thorlabs) to suppress the chromatic aberration. After removing the spectral components shorter than 1064 nm from the SC by combining a color filter (IR80, Kenko Optics) with a sharp long-pass filter (3RD1050LP, Omega Optical), the ω_1 and ω_2 laser pulses were superimposed by a notch filter (NF03-532/1064E-25, Semrock), and then introduced into a modified inverted microscope (ECLIPSE Ti-U, Nikon). Incident laser pulses were tightly focused onto a sample by the water-immersion objective lens (CFI Plan Apo 60 × NA 1.27, Nikon). The sample was placed on a piezoelectric stage (Nano-LP200, Mad City Lab) for microscopic imaging, and the CARS signal was collected by the dry objective lens (Plan S Fluor 40 × NA 0.6, Nikon), and was dispersed by the spectrometer (LS-785, Princeton Instruments). Finally, the CARS signal was detected by the CCD camera (Blaze 400-HR, Princeton Instruments).

2.2. Sample preparation

To confirm the performance of the developed system, polystyrene beads with a diameter of 10 μm (Polysciences Inc.) were used as test samples for CARS imaging. The original aqueous

OSA CONTINUUM

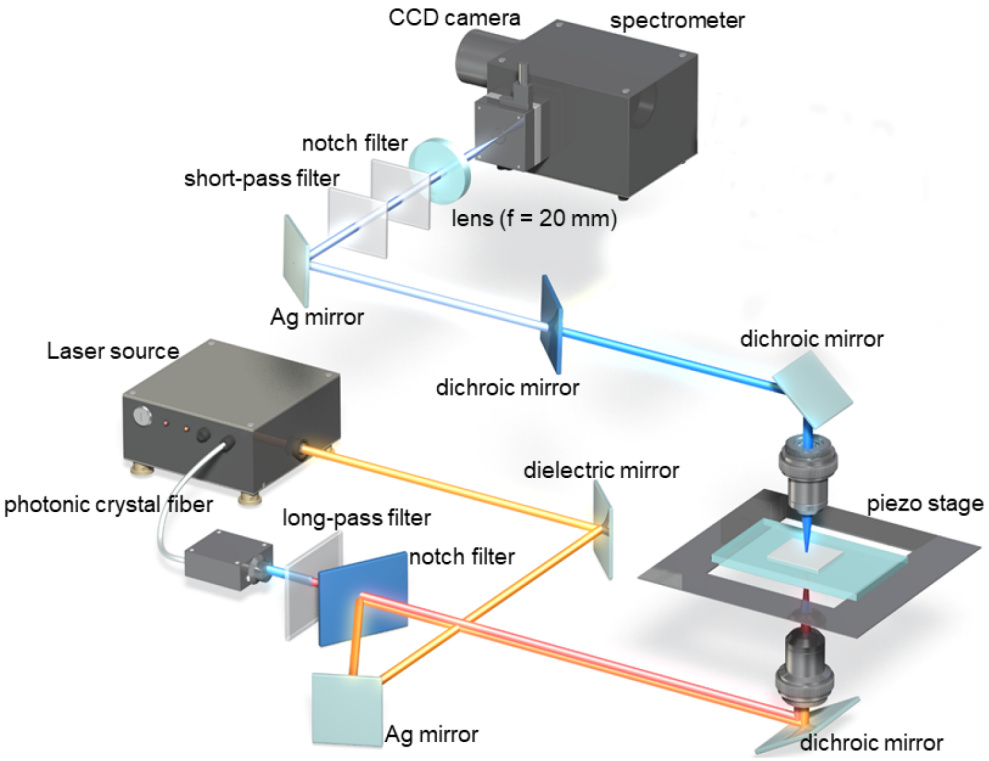

Fig. 1. Experimental setup of ultra-multiplex spectroscopic CARS system.

suspension of the beads was first diluted more than 10 times, and approximately 50 µL of the suspension was sandwiched between a coverslip and a slide glass.

A549 cells derived from a human lung adenocarcinoma were used as living cell samples. The cell line was demonstrated to synthesize lecithin and to contain a high concentration of unsaturated fatty acids [34]. Cells were plated on type collagen-coated chamber slides in Dulbecco's Modified Eagle's Medium supplemented with 10% fetal bovine serum and cultured for two days at 37 °C in a humidified incubator containing 5% CO_2 in air. Immediately before the measurements, the glass slide was removed from the chamber. The cells on the glass slide were covered with a coverslip, and then sealed with nail varnish. The input laser power at the sample position was set at ~80 mW and ~50 mW for ω_1 and ω_2, respectively. The total power (130 mW) of the laser source was less than that used in our previous study (200 mW) [32], partly because of the higher sensitivity of the CCD camera used in this study (PIXIS 100-BR-DDPIXIS 100-BR-DD (Princeton Instruments) was used in the previous living-cell imaging [32]). The pulse energies of the ω_1 and ω_2 pulses at the sample were approximately 100 and 65 nJ, respectively, corresponding to peak power of approximately 1.2 and 0.8 kW. We confirmed, through optical imaging, that the intensity of laser irradiation produced did not lead to substantial morphological changes in the cells.

3. Results and discussion

3.1. Ultra-multiplex CARS spectroscopic imaging of polystyrene beads

We evaluated the system by measuring the CARS signal of a polystyrene bead with a diameter of 10 µm. Figures 2(a) and (b) show the CARS spectra that were recorded by using the software

OSA CONTINUUM

to specify different exposure times, and the CARS signal at 1003 cm^{-1}, which corresponds to the vibrational mode associated with phenyl ring breathing, and its dependence on the exposure time that was set using the software. The laser source was MOFA, and the laser power for ω_1 and ω_2 was 10 mW and 50 mW, respectively. As we reported previously [32], the CARS signal was detected even when the exposure time was set to "0 ms" using the software. This is due to charge accumulation within the readout time. By extrapolating the results in Fig. 2(b), the effective exposure time by specifying an exposure time of "0 ms" using the software was evaluated to be approximately 0.8 ms. This value agrees well with the readout time of the CCD camera (~0.7 ms), which was output by the software. In addition to the CARS spectrum and image ("0-ms" exposure time) obtained using the MOFA laser source [32], in the present study, detailed evaluation of the effective exposure time is also presented.

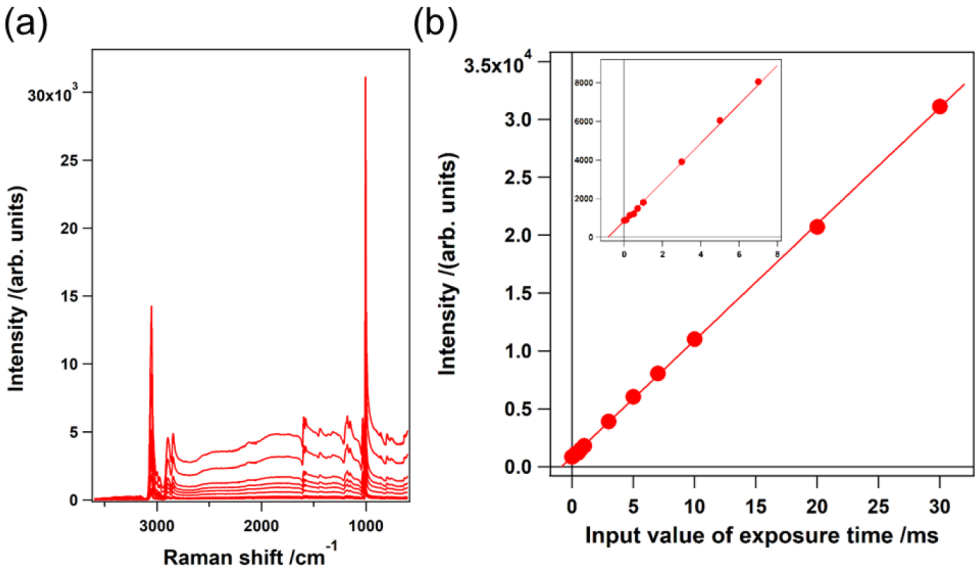

Fig. 2. CARS measurements using the MOFA laser source and the CCD camera with a fast readout time: (a) CARS spectra of a polystyrene bead (intensity uncorrected); (b) Dependence of the exposure time on the CARS signal (solid circles) at 1003 cm^{-1}, which corresponds to the vibrational mode associated with breathing of the phenyl ring and the fitted result (solid line).

Figure 3 shows the depth dependence of the CARS image at 1003 cm^{-1} obtained using the Q-switched microchip Nd:YAG laser source. The input laser power at the sample position was set to ~20 mW and ~8 mW for ω_1 and ω_2, respectively; this corresponds to peak power of approximately 0.8 and 0.3 kW, respectively. The size of each image was 161×161 pixels, and the total data-acquisition time was approximately 28 s. It should be emphasized that the results in Fig. 3 were obtained using a low-cost microchip laser source, while the MOFA laser was used in [32]. Based on the results of the present study, we confirmed that the passively Q-switched microchip Nd:YAG laser with a 33-kHz repetition rate can also be used for such high-speed measurements. By setting the exposure time to "0 ms" using the software, ultra-multiplex CARS imaging of the polystyrene bead was performed in the spectral range of 600–3600 cm^{-1} with a pixel dwell time of approximately 1 ms, which was limited mainly by the readout time of the CCD camera.

OSA CONTINUUM

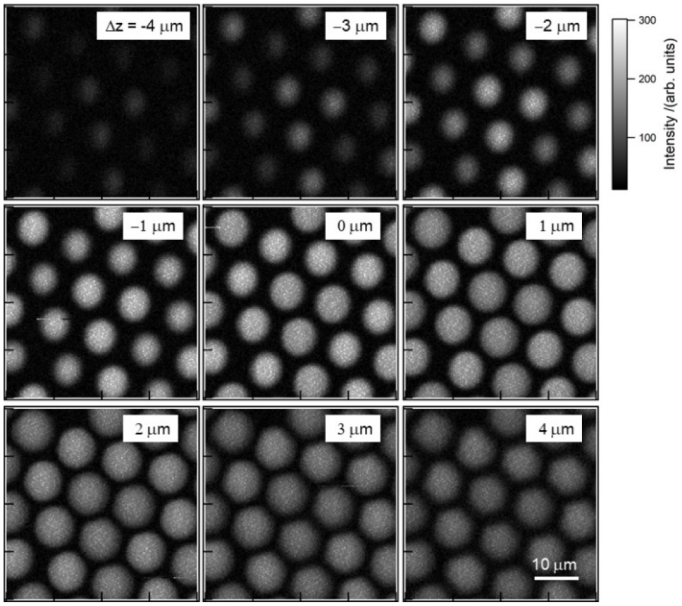

Fig. 3. CARS images in the phenyl-ring breathing vibrational mode (1003 cm^{-1}) at different depth positions; the images were obtained using the passively Q-switched microchip Nd:YAG laser and the CCD camera with a fast readout time. The exposure time was set to 0 ms using software. The resolution of image was 161 × 161 pixels, and the total data-acquisition time was approximately 28 s.

3.2. *Ultra-multiplex CARS spectroscopic imaging of living cells*

Figures 4(a) and (b) show an optical image of a living cell (A549) and the corresponding CARS image of the same cell. CARS imaging was performed using the combination of the MOFA laser source and the CCD camera with a fast readout time. The CARS image was mapped out simply by using the intensity of the raw CARS signal at the apparent peak position at 2850 cm^{-1}. The exposure time at each pixel was 10 ms. The sharp peak observed at 2850 cm^{-1} on the red spectrum in Fig. 4(c) corresponds to one of the bright spots inside the cell. As is well known, the band at approximately 2850 cm^{-1} corresponds to the CH_2 stretching vibrational mode, which is observed mainly in intracellular lipid droplets. A raw CARS signal consists of both a vibrationally resonant signal and so-called nonresonant background (NRB), which interfere with each other and produce dispersive line shapes (See Fig. 4(c)). We extracted the pure vibrationally resonant signal to obtain *spontaneous-Raman-equivalent* spectral profiles by performing numerical analysis using the maximum entropy method (MEM) [35]. The spectral profile of the pure vibrationally resonant signal, which corresponds to the imaginary part of $\chi^{(3)}$ ($\mathrm{Im}[\chi^{(3)}]$), is shown in Fig. 5. The main features of the spectral profiles in red and blue in Fig. 5 are in good agreement with those of intracellular lipids and proteins, respectively [36,37]. In particular, the characteristic Raman bands are indicated in Fig. 5; namely, the bands at 3427, 3200, 3066, 3017, 2930, 2854, 1744, 1657, 1451, 1438, 1303, 1265, and 1009 cm^{-1} correspond to the vibrational modes due to OH antisymmetric and symmetric stretching, aromatic CH stretching, =C-H stretching, CH_3 symmetric stretching, CH_2 symmetric stretching, C = O stretching, Amide I and/or *cis* C = C stretching, CH_3 degenerate deformation, CH_2 scissoring, and phenyl-ring breathing vibrational modes, respectively. A list of these vibrational modes has been reported elsewhere in part [32].

OSA CONTINUUM

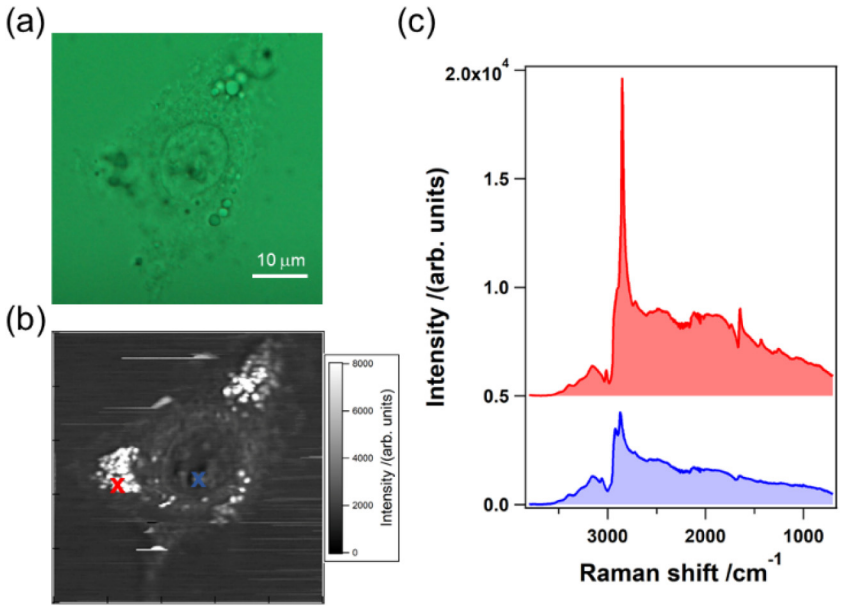

Fig. 4. (a) Optical image of an A549 cell; (b) CARS intensity mapping at 2850 cm^{-1}; (c) Spectral profiles of the raw CARS signal indicated at the two positions in (b) using red and blue crosses. The images were obtained using the MOFA laser source and a CCD camera with a fast readout time.

We analyzed the spectral profile in more detail by decomposing the Im[$\chi^{(3)}$] spectra into the sum of the Gaussian bands at each cell position. Figure 6 shows the typical fitted result of the intra-cellular-averaged Im[$\chi^{(3)}$] spectrum in the CH stretching region. In this study, we performed a more detailed analysis of the CH-stretching vibrational band when the analysis in [32]. Overall, the spectral profile was well fitted by seven Gaussian functions at 3017, 2953, 2939, 2921, 2902, 2872, and 2854 cm^{-1}. Based on the fitting procedure as shown in Fig. 6, ultra-multiplex spectroscopic CARS images are obtained. Figure 7 summarizes the results, where Figs. 7(a – r) show the CARS images at 3427, 3200, 3066, 3017, 2953, 2939, 2921, 2902, 2872, 2854, 1744, 1657, 1451, 1438, 1303, 1284, 1265, and 1009 cm^{-1}, respectively. The exposure time at each pixel was 10 ms. Because the CARS images at the vibrational bands at 2939 and 2921 cm^{-1} are similar to each other, and these bands are adjacent to each other, we considered the sum of the Gaussian bands at 2939 and 2921 cm^{-1} to be regarded as a single vibrational band (purple broken curve in Fig. 6). The vibrational bands in the present study were assigned by taking into account the CARS image contrast (see Fig. 7) and the literature values [38–46]. The results are summarized in Table 1. In the present study, we assume that the band at 2902 cm^{-1} is in the CH_2 anti-symmetric stretching mode.

The microscopic intracellular structures were visualized, as shown in Fig. 7. Particle-like structures with a diameter of a few micrometers were observed in the cytoplasm, as shown in Figs. 8(d), (j), (k), (n), (o), and (q). These bands are assigned as the C-H stretching vibrational mode of = C-H bonds (d), CH_2 symmetric stretching vibrational mode (j), C = O stretch mode of the ester (k), CH_2 scissoring mode (n), CH_2 twisting mode (o), and = C-H bending mode (q), all of which are typically observed for lipids. These organelles are, therefore, safely assigned as lipid droplets. As clearly shown in the CARS image (d) and (q), the lipid droplets contain rich unsaturated lipids. These results are consistent with the characteristics of the A549 cell, which is well known to produce unsaturated fats. On the other hand, the CARS image at 2939

OSA CONTINUUM

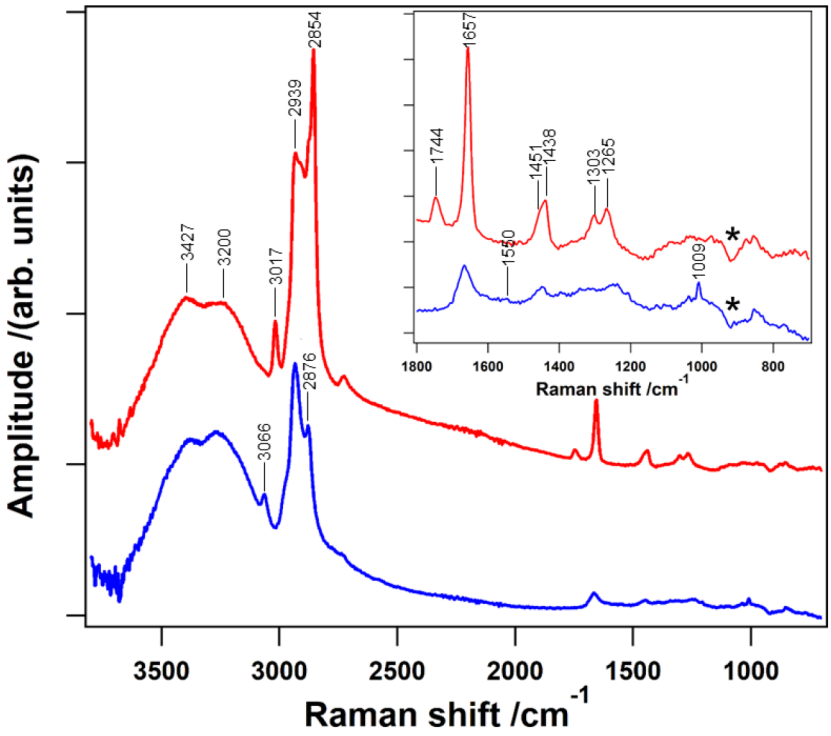

Fig. 5. Spontaneous-Raman-equivalent Im[$\chi^{(3)}$] spectra at the two intracellular positions indicated as red and blue crosses in Fig. 4(b). The inset shows enlarged spectral profiles in the fingerprint region. The dips indicated by "*" are artifacts due to the CARS spectral correction process, in which the CARS signal at each spatial point was divided by the nonresonant background of the coverslip underneath the suspension cell.

Table 1. Vibrational bands and their assignments for the intracellular Im[$\chi^{(3)}$] spectrum [38–46]

Typical Raman shift values(cm^{-1})	Assignment	Main molecular components
3427	O-H a-stretch.	Water
3200	O-H s-stretch.	Water
3066	C-H stretch.(aromatic)	Proteins
3017	=C-H stretch.	Lipids
2953	CH_3 a-stretch.	DNAs & RNAs
~2930	CH_3 s-stretch.	Proteins/Lipids
2902	CH_2 a-stretch.	Lipids/Proteins
2872	Overtone of CH_3 deform. in Fermi resonance with CH_3 s-stretch.	Proteins/Lipids
2854	CH_2 s-stretch.	Lipids
1744	C = O stretch. (ester)	Lipids
1657	*cis* C = C stretch./Amide I	Lipids/Proteins
~1550	Purine ring (adenine and guanine)	DNAs & RNAs
1451	CH_3 deg. deform.	Proteins
1438	CH_2 scis.	Lipids
1303	CH_2 twist.	Lipids
~1284	Amide III/C-H bend	Proteins
1265	=C-H bend.	Lipids
1004	Phenyl ring breath.	Proteins

Abbreviations: stretch.: stretching; deform.: deformation; rock.: rocking; twist.: twisting; scis.: scissors; bend.: bending; sym. or s- symmetric; anti. or a- antisymmetric; deg.: degenerate; breath.: breathing; Phe: phenylalanine.

OSA CONTINUUM

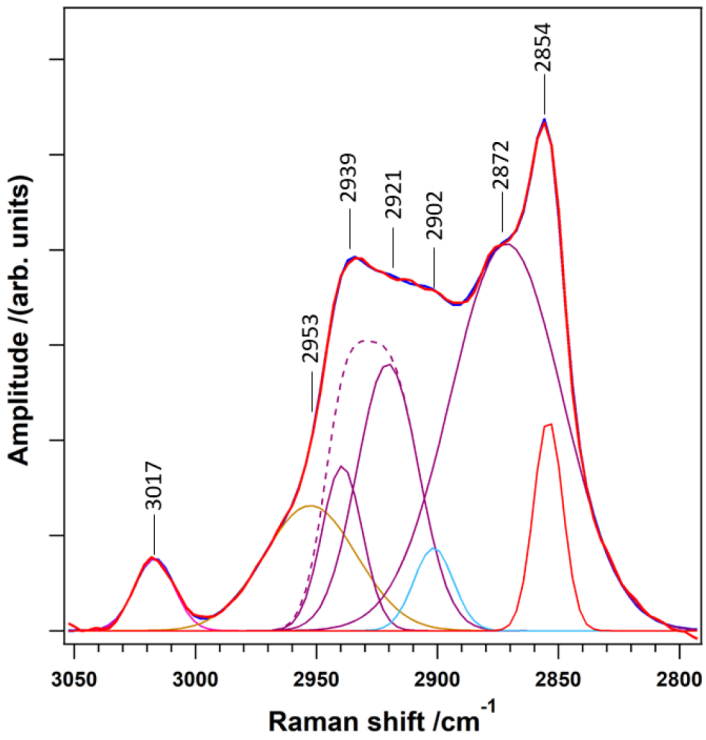

Fig. 6. Fitted results of the Im[$\chi^{(3)}$] spectrum in the CH stretching vibrational modes. Seven Gaussian functions centered at 2854, 2872, 2902, 2921, 2940, 2953, and 3017 cm^{-1} reproduced the experimentally obtained Im[$\chi^{(3)}$] spectrum well.

and 2921 cm^{-1} indicates a dark round structure in the cell. This corresponds to the cell nucleus. The intra-nuclear bright spots are assignable to the nucleolus, which introduces high vibrational contrast to the CARS images (c), (e), (f), (g), (i), (m), and (r). These vibrational modes correspond to the aromatic CH stretching (c), CH_3 asymmetric stretching (e), CH_3 symmetric stretching ((f) and (g)), overtone of CH_3 deformation in Fermi resonance with CH_3 symmetric stretching (i), CH_3 degenerate deformation (m), and phenyl ring breathing (r) vibrational modes, respectively. In our previous report on HeLa cells[32], the bands due to DNA and RNA were clearly observed, whereas the present results on A549 only exhibit weak signal intensity centered at 1550 cm^{-1}, probably due to cell-line dependence and the low signal-to-noise ratio in this study. In addition, the CARS image at 2902 cm^{-1} shows clear vibrational contrast at the nuclear membrane. We therefore assign the band at 2902 cm^{-1} as the CH_2 anti-symmetric vibrational mode due to phospholipids. On the other hand, the CARS images at 3427 and 3200 cm^{-1}, which correspond to OH stretching vibrational modes, have low contrast in the field of view.

In this study, we realized high-speed ultra-multiplex CARS imaging by performing live-cell imaging with an exposure time (on the software) of 1 ms using a combination of the MOFA laser source and a CCD camera with a fast readout time. Taking into account the finite readout time, the effective exposure time per pixel was estimated to be approximately 1.8 ms, which is a significant reduction compared to the previous study on living-cell imaging (exposure time per pixel: 50 ms) [32]. The improvement in the data-acquisition time was mainly due to the difference in the sensitivity and the readout speed of the CCD camera. The readout times in the present and the previous study [32] were 0.8 ms and ~3 ms, respectively. Figure 8 shows the result of the 200-μm^2 square (401 × 401 pixels) ultra-multiplex CARS spectroscopic imaging.

OSA CONTINUUM

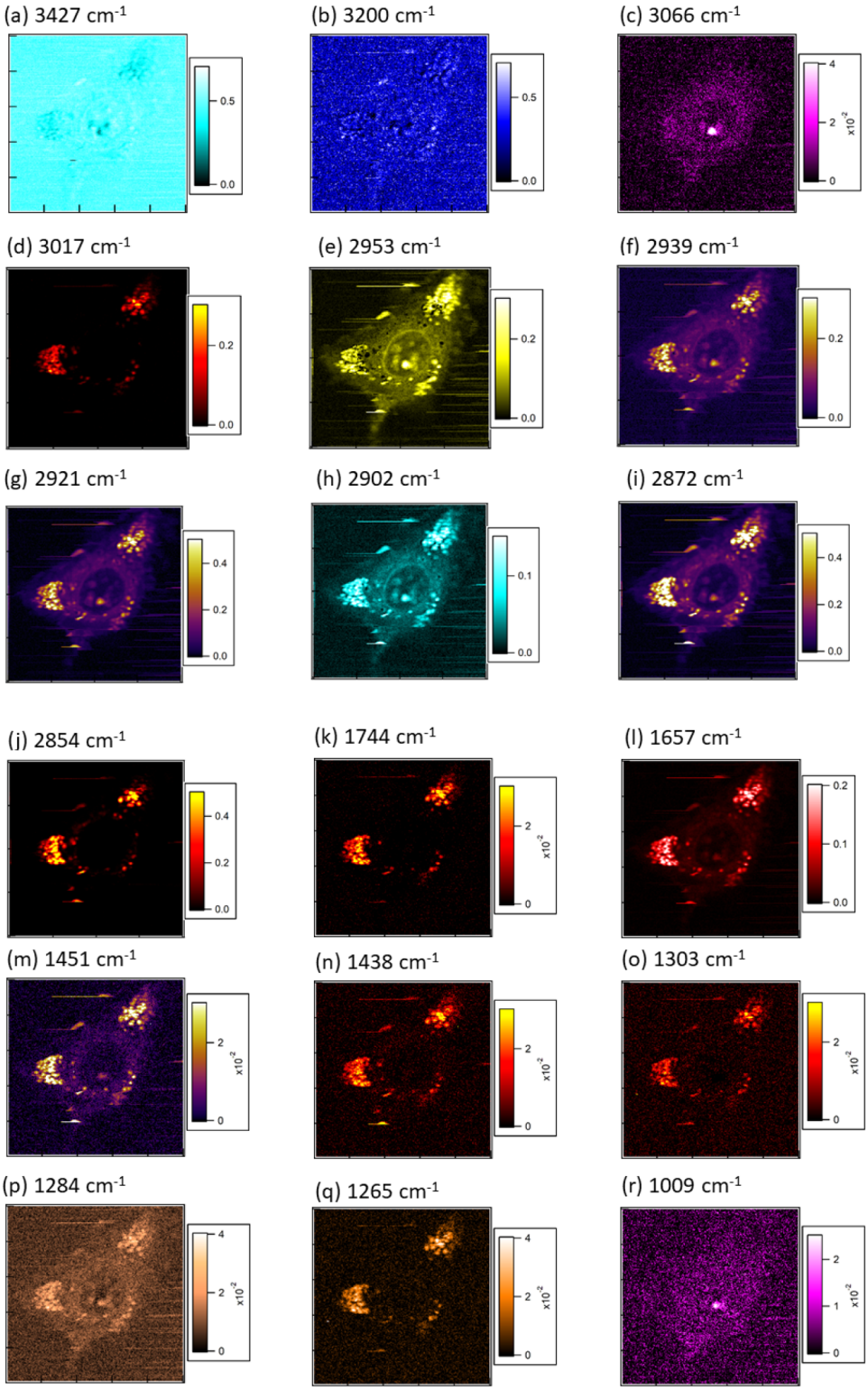

Fig. 7. CARS images of an A549 cell in G1 phase at (a) 3427, (b) 3200, (c) 3066, (d) 3017, (e) 2953, (f) 2939, (g) 2921, (h) 2902, (i) 2872, (j) 2854, (k) 1744, (l) 1657, (m) 1451, (n) 1438, (o) 1303, (p) l284, (q) 1265, and (r) 1009 cm^{-1}, respectively. The exposure time per pixel was 10 ms. The images were obtained using the MOFA laser source and the CCD camera with a fast readout time.

OSA CONTINUUM

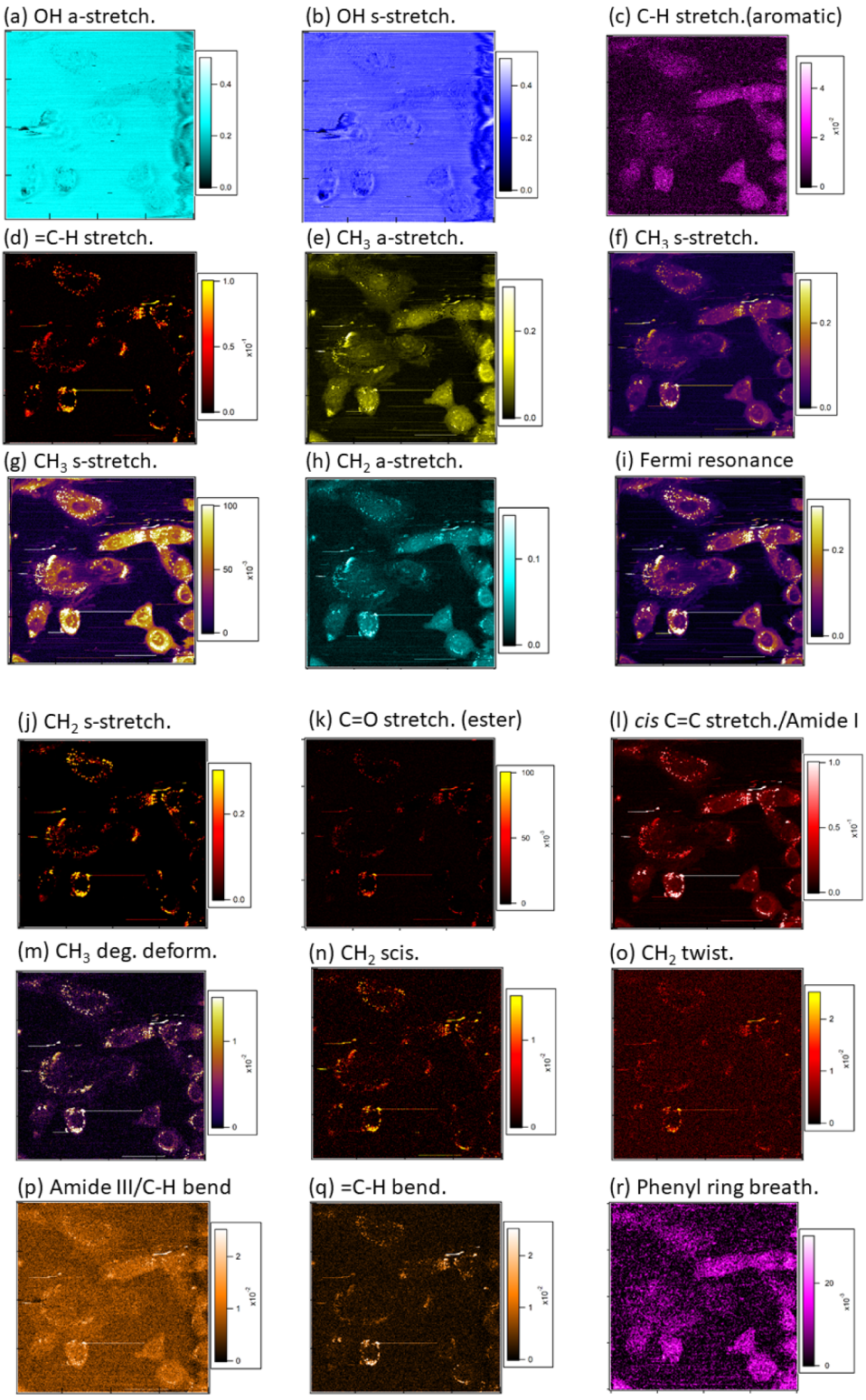

Fig. 8. CARS images of A549 cells at (a) 3427, (b) 3200, (c) 3066, (d) 3017, (e) 2953, (f) 2939, (g) 2921, (h) 2902, (i) 2872, (j) 2854, (k) 1744, (l) 1657, (m) 1451, (n) 1438, (o) 1303, (p) 1284, (q) 1265, and (r) 1009 cm^{-1}, respectively. The exposure time per pixel was ~1.8 ms. The images were obtained using the MOFA laser source and the CCD camera with a fast readout time.

OSA CONTINUUM

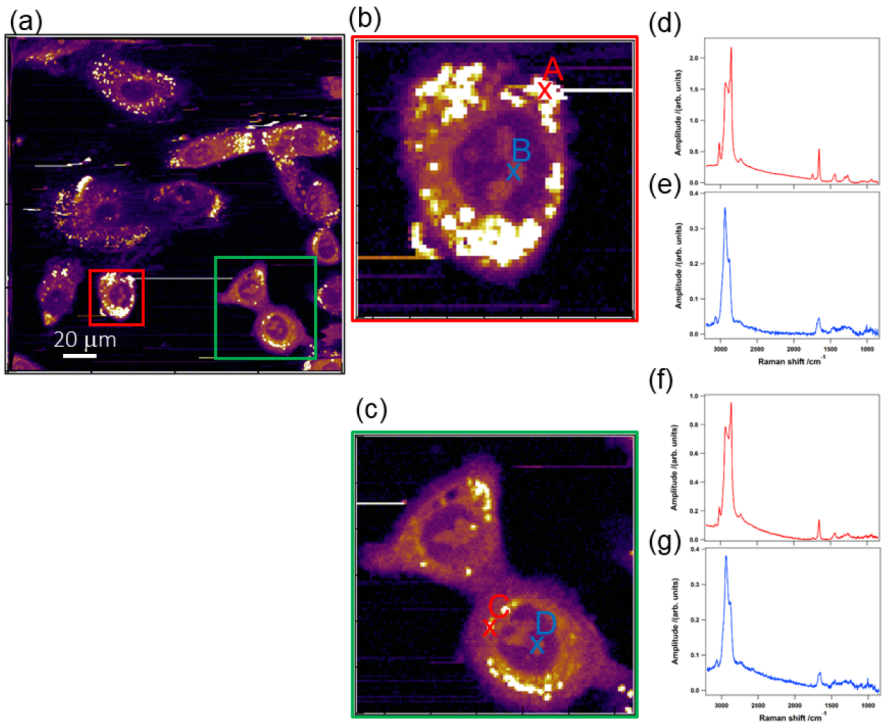

Fig. 9. (a) CARS image of A549 cells at 2939 cm^{-1} (the same as in Fig. 8(f)); Enlargements of the CARS images in the red (b) and green (c) boxes in (a); Im[$\chi^{(3)}$] spectra at position A (red cross in (b)) (d), B (blue cross in (b)) (e), C (red cross in (c)) (f), and D (blue cross in (c)) (g)

The spectral profiles of the Im[$\chi^{(3)}$] spectra are similar to those in Fig. 7. As clearly shown in Fig. 8, each cell is visualized using different vibrational contrast with an exposure time of approximately 1.8 ms per pixel. Figure 9 shows enlargements ((b) and (c)) and spectral profiles ((d-g)) of the images in Fig. 8. The red (Fig. 9(d) and (f)) and blue (Fig. 9(e) and (g)) spectral profiles in Fig. 9 show the 2-μm^2-spatially averaged Im[$\chi^{(3)}$] spectra, which are assignable to unsaturated lipids and proteins, respectively. The use of an effective exposure time of ~1.8 ms enabled us to perform ultra-multiplex CARS imaging of living cells.

4. Conclusion

In this study, we performed ultra-multiplex CARS spectroscopic imaging using a CCD camera with a high-speed readout time. The exposure time was reduced to 0.8 ms, limited by the readout time of the CCD camera. CARS images (with resolution of 161×161 pixels) of polymer beads were obtained with the total data-acquisition time of approximately 28 s, despite the use of a low-cost microchip laser source. Based on the clear molecular fingerprint, we successfully visualized intracellular molecular distribution with more than 15 vibrational bands with an effective exposure time of 1.8 ms using the MOFA laser source. The combination of this visualization technique with multivariate analysis methods, such as multivariate curve resolution-alternating least-square (MCR-ALS) [47], can help researchers gain meaningful insights into the dynamics of intracellular metabolic activity. Our label-free imaging presents considerable potential for miniaturized, non-invasive, real-time, and cellular-level molecular diagnostics for experimental and clinical applications.

OSA CONTINUUM

Funding

Japan Society for the Promotion of Science (JSPS) (18H02000); Konica Minolta Imaging Science Foundation.

Acknowledgments

The authors gratefully acknowledge the assistance of J. Ukon of Ukon Craft Science, Ltd. with establishing this fruitful collaboration between Japanese and French laboratories. The authors thank Princeton Instruments for providing the Blaze, a new type of CCD camera that enabled us to perform ultra-multiplex (600-3600 cm^{-1}) CARS spectroscopic imaging in the fastest recorded time.

Disclosures

The authors declare that there are no conflicts of interest related to the work in this article.

References

1. J. X. Cheng and X. S. Xie, "Vibrational spectroscopic imaging of living systems: An emerging platform for biology and medicine," Science **350**(6264), aaa8870 (2015).
2. H. Kano, "Molecular Spectroscopic Imaging Using a White-Light Laser Source," Bull. Chem. Soc. Jpn. **83**(7), 735–743 (2010).
3. C. Zhang and J.-X. Cheng, "Perspective: Coherent Raman scattering microscopy, the future is bright," APL Photonics **3**(9), 090901 (2018).
4. L. Wei, Z. Chen, L. Shi, R. Long, A. V. Anzalone, L. Zhang, F. Hu, R. Yuste, V. W. Cornish, and W. Min, "Super-multiplex vibrational imaging," Nature **544**(7651), 465–470 (2017).
5. J. P. R. Day, K. F. Domke, G. Rago, H. Kano, H. Hamaguchi, E. M. Vartiainen, and M. Bonn, "Quantitative Coherent Anti-Stokes Raman Scattering (CARS) Microscopy," J. Phys. Chem. B **115**(24), 7713–7725 (2011).
6. W. Min, C. W. Freudiger, S. J. Lu, and X. S. Xie, "Coherent Nonlinear Optical Imaging: Beyond Fluorescence Microscopy," Annu. Rev. Phys. Chem. **62**(1), 507–530 (2011).
7. C. Y. Chung, J. Boik, and E. O. Potma, "Biomolecular Imaging with Coherent Nonlinear Vibrational Microscopy," Annu. Rev. Phys. Chem. **64**(1), 77–99 (2013).
8. C. S. Liao and J. X. Cheng, "In Situ and In Vivo Molecular Analysis by Coherent Raman Scattering Microscopy," Annu. Rev. Anal. Chem. **9**(1), 69–93 (2016).
9. C. H. Camp Jr and M. T. Cicerone, "Chemically sensitive bioimaging with coherent Raman scattering," Nat. Photonics **9**(5), 295–305 (2015).
10. J. X. Cheng, A. Volkmer, L. D. Book, and X. S. Xie, "Multiplex coherent anti-stokes Raman scattering microspectroscopy and study of lipid vesicles," J. Phys. Chem. B **106**(34), 8493–8498 (2002).
11. M. Muller and J. M. Schins, "Imaging the thermodynamic state of lipid membranes with multiplex CARS microscopy," J. Phys. Chem. B **106**(14), 3715–3723 (2002).
12. T. W. Kee and M. T. Cicerone, "Simple approach to one-laser, broadband coherent anti-Stokes Raman scattering microscopy," Opt. Lett. **29**(23), 2701–2703 (2004).
13. H. Kano and H. Hamaguchi, "Ultrabroadband (> 2500 cm(-1)) multiplex coherent anti-Stokes Raman scattering microspectroscopy using a supercontinuum generated from a photonic crystal fiber," Appl. Phys. Lett. **86**(12), 121113 (2005).
14. G. I. Petrov and V. V. Yakovlev, "Enhancing red-shifted white-light continuum generation in optical fibers for applications in nonlinear Raman microscopy," Opt. Express **13**(4), 1299–1306 (2005).
15. E. R. Andresen, H. N. Paulsen, V. Birkedal, J. Thogersen, and S. R. Keiding, "Broadband multiplex coherent anti-Stokes Raman scattering microscopy employing photonic-crystal fibers," J. Opt. Soc. Am. B **22**(9), 1934–1938 (2005).
16. C. H. Camp Jr., Y. J. Lee, J. M. Heddleston, C. M. Hartshorn, A. R. Hight Walker, J. N. Rich, J. D. Lathia, and M. T. Cicerone, "High-Speed Coherent Raman Fingerprint Imaging of Biological Tissues," Nat. Photonics **8**(8), 627–634 (2014).
17. C. W. Freudiger, W. Min, G. R. Holtom, B. Xu, M. Dantus, and X. S. Xie, "Highly specific label-free molecular imaging with spectrally tailored excitation stimulated Raman scattering (STE-SRS) microscopy," Nat. Photonics **5**(2), 103–109 (2011).
18. Y. Ozeki, W. Umemura, Y. Otsuka, S. Satoh, H. Hashimoto, K. Sumimura, N. Nishizawa, K. Fukui, and K. Itoh, "High-speed molecular spectral imaging of tissue with stimulated Raman scattering," Nat. Photonics **6**(12), 845–851 (2012).
19. C.-S. Liao, K.-C. Huang, W. Hong, A. J. Chen, C. Karanja, P. Wang, G. Eakins, and J.-X. Cheng, "Stimulated Raman spectroscopic imaging by microsecond delay-line tuning," Optica **3**(12), 1377 (2016).

OSA CONTINUUM

20. T. Hellerer, A. M. K. Enejder, and A. Zumbusch, "Spectral focusing: High spectral resolution spectroscopy with broad-bandwidth laser pulses," Appl. Phys. Lett. **85**(1), 25–27 (2004).
21. J. P. Ogilvie, E. Beaurepaire, A. Alexandrou, and M. Joffre, "Fourier-transform coherent anti-Stokes Raman scattering microscopy," Opt. Lett. **31**(4), 480–482 (2006).
22. K. Hashimoto, M. Takahashi, T. Ideguchi, and K. Goda, "Broadband coherent Raman spectroscopy running at 24,000 spectra per second," Sci. Rep. **6**(1), 21036 (2016).
23. K. Hashimoto, J. Omachi, and T. Ideguchi, "Ultra-broadband rapid-scan Fourier-transform CARS spectroscopy with sub-10-fs optical pulses," Opt. Express **26**(11), 14307–14314 (2018).
24. T. Ideguchi, S. Holzner, B. Bernhardt, G. Guelachvili, N. Picque, and T. W. Hansch, "Coherent Raman spectro-imaging with laser frequency combs," Nature **502**(7471), 355–358 (2013).
25. M. Okuno, H. Kano, P. Leproux, V. Couderc, J. P. R. Day, M. Bonn, and H. Hamaguchi, "Quantitative CARS Molecular Fingerprinting of Single Living Cells with the Use of the Maximum Entropy Method," Angew. Chem. Int. Edit. **49**(38), 6773–6777 (2010).
26. K. Isobe, A. Suda, M. Tanaka, H. Hashimoto, F. Kannari, H. Kawano, H. Mizuno, A. Miyawaki, and K. Midorikawa, "Single-pulse coherent anti-Stokes Raman scattering microscopy employing an octave spanning pulse," Opt. Express **17**(14), 11259–11266 (2009).
27. H. Segawa, M. Okuno, H. Kano, P. Leproux, V. Couderc, and H. Hamaguchi, "Label-free tetra-modal molecular imaging of living cells with CARS, SHG, THG and TSFG (coherent anti-Stokes Raman scattering, second harmonic generation, third harmonic generation and third-order sum frequency generation)," Opt. Express **20**(9), 9551–9557 (2012).
28. H. Segawa, Y. Kaji, P. Leproux, V. Couderc, T. Ozawa, T. Oshika, and H. Kano, "Multimodal and multiplex spectral imaging of rat cornea ex vivo using a white-light laser source," J. Biophotonics **8**(9), 705–713 (2015).
29. C. Lefort, R. P. O'Connor, V. Blanquet, L. Magnol, H. Kano, V. Tombelaine, P. Leveque, V. Couderc, and P. Leproux, "Multicolor multiphoton microscopy based on a nanosecond supercontinuum laser source," J. Biophotonics **9**(7), 709–714 (2016).
30. R. Vlijm, X. Li, M. Panic, D. Ruthnick, S. Hata, F. Herrmannsdorfer, T. Kuner, M. Heilemann, J. Engelhardt, S. W. Hell, and E. Schiebel, "STED nanoscopy of the centrosome linker reveals a CEP68-organized, periodic rootletin network anchored to a C-Nap1 ring at centrioles," Proc. Natl. Acad. Sci. U. S. A. **115**(10), E2246–E2253 (2018).
31. T. Akiyama, A. Inoko, Y. Kaji, S. Yonemura, K. Kakiguchi, H. Segawa, K. Ishitsuka, M. Yoshida, O. Numata, P. Leproux, V. Couderc, T. Oshika, and H. Kano, "SHG-specificity of cellular Rootletin filaments enables naive imaging with universal conservation," Sci. Rep. **7**(1), 39967 (2017).
32. H. Yoneyama, K. Sudo, P. Leproux, V. Couderc, A. Inoko, and H. Kano, "CARS molecular fingerprinting using sub-100-ps microchip laser source with fiber amplifier," APL Photonics **3**(9), 092408 (2018).
33. M. Okuno, H. Kano, P. Leproux, V. Couderc, and H. Hamaguchi, "Quantitative coherent anti-Stokes Raman scattering microspectroscopy using a nanosecond supercontinuum light source," Opt. Fiber Technol. **18**(5), 388–393 (2012).
34. M. Lieber, G. Todaro, B. Smith, A. Szakal, and W. Nelson-Rees, "A continuous tumor-cell line from a human lung carcinoma with properties of type II alveolar epithelial cells," Int. J. Cancer **17**(1), 62–70 (1976).
35. E. M. Vartiainen, H. A. Rinia, M. Müller, and M. Bonn, "Direct extraction of Raman line-shapes from congested CARS spectra," Opt. Express **14**(8), 3622–3630 (2006).
36. H. W. Wu, J. V. Volponi, A. E. Oliver, A. N. Parikh, B. A. Simmons, and S. Singh, "In vivo lipidomics using single-cell Raman spectroscopy," Proc. Natl. Acad. Sci. U. S. A. **108**(9), 3809–3814 (2011).
37. D. Fu, F. K. Lu, X. Zhang, C. Freudiger, D. R. Pernik, G. Holtom, and X. S. Xie, "Quantitative Chemical Imaging with Multiplex Stimulated Raman Scattering Microscopy," J. Am. Chem. Soc. **134**(8), 3623–3626 (2012).
38. T. Shimanouchi, "Tables of molecular vibrational frequencies. Consolidated volume II," J. Phys. Chem. Ref. Data **6**(3), 993–1102 (1977).
39. Q. Matthews, A. Brolo, J. Lum, X. Duan, and A. Jirasek, "Raman spectroscopy of single human tumour cells exposed to ionizing radiation in vitro," Phys. Med. Biol. **56**(1), 19–38 (2011).
40. M. T. Cicerone and C. H. Camp, "Histological coherent Raman imaging: a prognostic review," Analyst **143**(1), 33–59 (2018).
41. C. Krafft, L. Neudert, T. Simat, and R. Salzer, "Near infrared Raman spectra of human brain lipids," Spectrochim. Acta, Part A **61**(7), 1529–1535 (2005).
42. B. W. Barry, H. G. M. Edwards, and A. C. Williams, "Fourier transform Raman and infrared vibrational study of human skin: Assignment of spectral bands," J. Raman Spectrosc. **23**(11), 641–645 (1992).
43. H. Deng, V. A. Bloomfield, J. M. Benevides, and G. J. Thomas, "Dependence of the Raman signature of genomic B-DNA on nucleotide base sequence," Biopolymers **50**(6), 656–666 (1999).
44. R. G. Snyder, H. L. Strauss, and C. A. Elliger, "Carbon-hydrogen stretching modes and the structure of n-alkyl chains. 1. Long, disordered chains," J. Phys. Chem. **86**(26), 5145–5150 (1982).
45. R. G. Snyder and J. R. Scherer, "Band structure in the C–H stretching region of the Raman spectrum of the extended polymethylene chain: Influence of Fermi resonance," J. Chem. Phys. **71**(8), 3221–3228 (1979).
46. K. G. Brown, E. Bicknell-Brown, and M. Ladjadj, "Raman-active bands sensitive to motion and conformation at the chain termini and backbones of alkanes and lipids," J. Phys. Chem. **91**(12), 3436–3442 (1987).
47. M. Ando and H. Hamaguchi, "Molecular component distribution imaging of living cells by multivariate curve resolution analysis of space-resolved Raman spectra," J. Biomed. Opt. **19**(1), 011016 (2014).